JOURNAL OF SPACECRAFT AND ROCKETS
Vol. 43, No. 3, May–June 2006

Optimal Deployment/Retrieval of a Tethered Formation Spinning in the Orbital Plane

Paul Williams*
Royal Melbourne Institute of Technology University, Melbourne, Victoria 3083, Australia

The deployment/retrieval of a spinning three-mass tethered formation is considered. The tethered formation is modeled by point mass satellites connected via inelastic tethers. Optimal deployment/retrieval trajectories using tension control are determined for different spin conditions. Deployment and retrieval trajectories are obtained that maintain the tether spin at the desired rate and keep the system in the desired physical arrangement at the end of deployment/retrieval. Parametric studies of the effect of system spin rate and maneuver time are performed. Numerical results show that it is necessary to constrain the relative tether geometry to prevent any two tethers crossing each other. It is also shown that the tether spin rate tends to decrease during deployment but can be restored to the desired value by overdeploying the tethers and then reeling them in rapidly. Numerical results also illustrate the symmetrical nature of deployment and retrieval.

Nomenclature

$\boldsymbol{e}$	=	initial and terminal constraint functions for optimal control problem
$\mathcal{E}$	=	Mayer component of cost function in optimal control problem
$\boldsymbol{f}$	=	system state equations
$\mathcal{J}$	=	cost function in optimal control problem
k_{1_j}	=	proportional feedback gain for length feedback for jth tether
k_{2_j}	=	derivative feedback gain for length feedback for jth tether
L	=	reference tether length, m
$\mathcal{L}$	=	integrand in Bolza component of cost function in optimal control problem
l_j	=	length of jth tether, m
m	=	total system mass ($m_1 + m_2 + m_3$), kg
m_j	=	mass of the jth satellite, kg
Q_{q_j}	=	generalized force for q_j coordinate in Lagrange's equations
R_O	=	orbit radius of the system center of mass, m
r_j	=	position vector of the jth satellite in orbital frame relative to the system center of mass (x_j, y_j), m
T_j	=	tension in the jth tether, N
$\mathcal{T}$	=	system kinetic energy, J
u_j	=	nondimensional tension in jth tether ($T_j/[m\omega^2 L]$)
u_{0_j}	=	nondimensional tension for zero-length acceleration of jth tether
$\mathcal{V}$	=	system potential energy, J
$\boldsymbol{x}$	=	system-state vector
Λ_{c_j}	=	nondimensional commanded length of jth tether
Λ_j	=	nondimensional tether length of jth tether
θ_j	=	in-plane libration angle of the jth tether, rad
μ	=	gravitational constant of the Earth, km^3/s^2
μ_j	=	mass ratio of the jth satellite to total system mass (m_j/m)
τ	=	nondimensional time (ωt), rad
ω	=	orbital angular velocity of the system center of mass, rad/s

Superscripts

$\dot{(\,)}$	=	time derivative $\mathrm{d}(\,)/\mathrm{d}t$
$(\,)'$	=	nondimensional time derivative $\mathrm{d}(\,)/\mathrm{d}(\omega t)$

Introduction

SPACECRAFT formation flying has generated a lot of interest in recent years, primarily because it promises to revolutionize the collection of scientific data from space. Flying spacecraft in formation is very challenging because of long-term perturbation effects that not only require accurate state determination but also efficient and reliable control systems. The advantages of flying multiple spacecraft in close proximity for space interferometry has led to proposals for several different configurations. Leitner et al.[1] discuss the possible approaches to the configuration design of large space apertures for space interferometry. The most basic approach is to use a monolithic structure, such as that used by the Hubble Space Telescope. However, single collecting surfaces such as these are limited by the availability of launch vehicles (i.e., the structure must fit into the cargo bay of the launch vehicle). Although these types of structures are preferable to more exotic arrangements from an engineering point of view, future scientific requirements demand much better image resolutions and therefore larger apertures than can be provided by such structures. The Next Generation Space Telescope will use a filled deployable aperture, allowing increased resolution at lower risk than that perceived for the use of sparse apertures. To achieve very sparse apertures, deployable booms have been considered. However, for even greater precision, long booms become impractical, and focus has been shifted toward the use of tethers. For example, the Submillimeter Probe of the Evolution of Cosmic Structure mission proposed for the 2015 timeframe may use a spinning tethered constellation placed at the sun–Earth L_2 point to take interferometric measurements. Tethered configurations require rotation to provide a centrifugal stiffening effect, and careful control and monitoring of the tether vibrations is necessary to position the spacecraft with the desired precision. Alternatively, free-flying spacecraft can be used to generate a spacecraft formation. This approach trades the uncertainties of using flexible structures such as tethers for fuel consumption.

Although significant research has been undertaken to study the motion and control of tethered two-body systems,[2] comparatively few studies have been presented on the dynamics and control of tethered formations. Misra et al.[3] studied the dynamics of an open three-mass tethered system for both constant and variable length tethers. The equilibrium and stability of these systems was studied in more detail by Misra,[4] who also showed that the integral of motion

Received 10 April 2005; revision received 21 August 2005; accepted for publication 24 August 2005.

*Research Fellow, School of Aerospace, Mechanical, and Manufacturing Engineering; paul.williams@rmit.edu.au. Member AIAA.

of the system is given by the Hamiltonian of the system per unit mass. Four configurations of equilibrium are known to exist: two where the masses are triangular, and two where the masses are collinear. The triangular configurations are unstable, whereas the collinear configurations are stable.

Tan and Bainum[5] considered the control of an in-plane tethered constellation for auroral observation missions. In their analysis, two spacecraft were connected by tethers via a central hub, which was the approximate location of the orbit of the system center of mass. Orbit control of the system was assumed to be applied using methods presented in other papers, and the control strategy was reduced to controlling the tether librations. Although the control strategy takes into account the electric circuitry used to reel the tethers, the configuration is not closed and so the applicability of the control approach for more general spinning configurations is questionable. Furthermore, only a linear control strategy was discussed, which may have limitations when applied to spinning tethered constellations.

Farley and Quinn[6] discussed the future of tethered formation flying for interferometry and separated configurations into open (pendulum-type) and closed (triangular-type) arrangements. Sedwick and Schweighart[7] considered various methods for controlling the positions of an array of sparse apertures. Different configurations of satellites were considered such as tethered triangle and hub-and-spoke arrangements, as well as electromagnetically coupled apertures. The transfer of momentum among the satellites was considered through the use of reaction wheels and tether reeling or the use of electromagnetic forces and reaction wheels. It was suggested that electromagnetically coupled systems allow greater mobility of the satellites than that provided by tethers.

Quadrelli[8] developed a sophisticated mathematical model for tethered satellite formations including orbital perturbations, thermal effects, and tether flexibility. The tether was modeled using a lumped-mass discretization. Variable length tethers were handled by appropriate convective terms in the equations of motion. Quadrelli[9] later used a steady-state linear quadratic regulator (LQR) to control the motion of the spacecraft in the formation. In this control approach, the system dynamics are linearized and a quadratic performance index containing weighted state deviations and controls is minimized over an infinite horizon. The dynamics of linear tethered interferometers (three masses connected linearly via tethers) has received some attention for use in deep-space interferometry.[10,11] Bombardelli et al.[12] studied the dynamics of a spinning linear interferometer in an Earth-trailing heliocentric orbit. They found that solar-radiation pressure and thermal variations are the most dominant perturbations on the system, causing either lateral vibrations or length excitations. A higher spin velocity is desirable from the point of view of stability. Bombardelli et al.[13] studied the influence of solar-radiation pressure on a spinning linear interferometer. They derived an analytical expression for the solar pressure force on a cylindrical tether with arbitrary orientation. The effect of this pressure on the lateral modes of a tethered interferometer was determined and found to give rise to very low-frequency oscillations of the central member of the configuration (on the orders of millimeters). Changing the plane of rotation of such a system was considered by Bombardelli et al.[14] Kim and Hall[15] have studied the dynamics of a tethered interferometer arrangement designed for the Submillimeter Probe of the Evolution of Cosmic Structure mission[16] and developed a controller using thruster inputs to control the configuration. The static shape of a spinning tethered interferometer was first studied by DeCou,[17] who ignored the effects of external disturbances such as gravity-gradient forces and solar pressure.

Cosmo et al.[18] considered the design requirements for a low-Earth-orbit demonstrator mission for a tethered interferometer to minimize the perturbations due to Earth's oblateness and to provide nearly constant thermal inputs. Dynamic simulations were carried out using a lumped-mass model with realistic environmental inputs. Preliminary investigation of a deployment procedure was also conducted for two cases: 1) where the tether is spun initially using thrusters and then deployed, and 2) where the system is deployed and then spun. The first scenario is more desirable because of the larger tension induced by the spin.

The dynamics of tethered formations in low Earth orbit has also received attention in recent years. Williams and Moore[19] studied the dynamics of Earth-facing tethered constellations kept taut by spinning the tether around the nadir-pointing line. It was suggested that medium spin rates (i.e., where the tether spin rate is comparable to the orbital angular velocity) are the most suitable for Earth-observation missions. To keep the system nadir pointing, a torque must be applied in the velocity direction. Two methods were investigated for generating the required torque: electromagnetic torquing and utilization of the gravity gradient in combination with a three-dimensional configuration. Tragesser[20] and Tragesser and Tuncay[21] studied tethered formations for terrestrial observation missions. Tragesser[20] studied a planar triangular configuration and found no stable configuration in the presence of tether flexibility, whereas Tragesser and Tuncay[21] considered fully three-dimensional configurations and found particular configurations that were stable.

Pizarro-Chong and Misra[22] studied the dynamics of tethered constellations for both open- and closed-hub-and-spoke configurations. The system was modeled using point masses connected via straight but elastic tethers. The equations of motion, formulated via Lagrange's equations, were derived for the cases where the system spins in the orbital plane and when the system spins normal to the orbital plane. Numerical simulation results illustrate the stability of different system configurations. It was found that, for a circular orbit with more than four bodies, the configuration must be closed and spinning to provide stability.

Nakaya et al.[23] considered the deployment of a tethered constellation in a circular low Earth orbit using a virtual structure architecture. The tethered system was modeled as three rigid bodies connected via tethers represented by lumped masses. Deployment profiles were determined either as functions of the system angular momentum or tether tension. Control of the system angular momentum was achieved using thrusters on the satellites.

Control of single tether systems has been studied for a wide range of cases including such essential features as deployment and retrieval[24–26] and for more advanced scenarios such as payload capture.[27,28] In most of these studies, control of the system via tether tension has been sought. Control of tethered formations in low Earth orbit using similar approaches has not been addressed previously. The purpose of this paper is to apply optimal control methodology to the deployment and retrieval phases of a spinning tethered constellation. The equations of motion and results are presented in nondimensional form, allowing some general conclusions to be drawn. The system is assumed to consist of point masses connected via inelastic straight tethers and to be spinning within the orbital plane. In the realm of low Earth orbits, the system is subject to gravity gradient and Coriolis effects, which allows control of the tether spin rate by appropriate reeling of the tethers. This is the main novelty of the current work, which demonstrates that differential length rates can generate sufficient Coriolis forces to adequately control the system without resorting to tangential thrusting to maintain the desired spin rate at the beginning and end of deployment/retrieval.

Mathematical Model

It has been common practice in control-system design to employ suitable low-order models of a dynamic system for preliminary control design. For example, for single-tethered satellite systems, an inextensible tether model is often employed and has been shown to generate good results with respect to more accurate models of the system. To study the deployment and retrieval phases of a tethered formation, a simplified model of the system is used. To allow for control via tension control, the system is modeled as a set of point masses connected via inelastic, massless tethers. For simplicity, only a three-mass triangular configuration is considered here.

The tether formation considered in this paper is shown in Fig. 1. An orbital coordinate system is used to represent the dynamics, the origin of which is at the system c.m. O. The x axis points positively outward from the center of the Earth along the local vertical, and the y axis points in the direction of the orbit-velocity vector. Because the motion is referenced relative to the c.m., the system is completely characterized by four coordinates. The generalized coordinates are

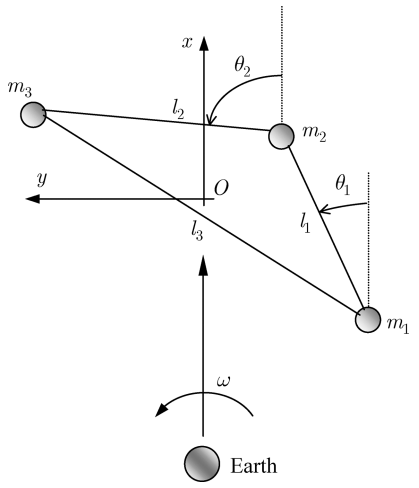

Fig. 1 Tethered formation control model (not to scale).

selected as the lengths of the tethers connecting masses m_1 and m_2 (l_1) and m_2 and m_3 (l_2), and the corresponding angles of those tethers relative to the local vertical (θ_1 and θ_2).

The c.m. constraint is represented by

$$\sum_{j=1}^{3} m_j \boldsymbol{r}_j = 0 \tag{1}$$

where $\boldsymbol{r}_j = (x_j, y_j)$ is the position vector of the jth mass relative to the center of mass in the orbital frame. In addition to Eq. (1), the geometric relations between the generalized coordinates and the Cartesian coordinates are given by

$$x_2 = x_1 + l_1 \cos\theta_1, \qquad x_3 = x_2 + l_2 \cos\theta_2$$
$$y_2 = y_1 + l_1 \sin\theta_1, \qquad y_3 = y_2 + l_2 \sin\theta_2 \tag{2}$$

After combining Eqs. (1) and (2), one obtains

$$\begin{bmatrix} x_1 \\ x_2 \\ x_3 \end{bmatrix} = [A] \begin{bmatrix} l_1 \cos\theta_1 \\ l_2 \cos\theta_2 \end{bmatrix}, \qquad \begin{bmatrix} y_1 \\ y_2 \\ y_3 \end{bmatrix} = [A] \begin{bmatrix} l_1 \sin\theta_1 \\ l_2 \sin\theta_2 \end{bmatrix} \tag{3}$$

where

$$[A] = \begin{bmatrix} -(\mu_2 + \mu_3) & -\mu_3 \\ \mu_1 & -\mu_3 \\ \mu_1 & \mu_1 + \mu_2 \end{bmatrix} \tag{4}$$

and $\mu_j \triangleq m_j/(m_1 + m_2 + m_3)$ are the nondimensional masses of the satellites. The kinetic energy of the system can be expressed in the following form[3]:

$$\mathcal{T} = \frac{1}{2} \sum_{j=1}^{3} m_j (\dot{\boldsymbol{R}}_O + \dot{\boldsymbol{r}}_j) \cdot (\dot{\boldsymbol{R}}_O + \dot{\boldsymbol{r}}_j) = \frac{1}{2} \Bigg[(m_1 + m_2 + m_3) \times \dot{\boldsymbol{R}}_O \cdot \dot{\boldsymbol{R}}_O + 2\dot{\boldsymbol{R}}_O \cdot \sum_{j=1}^{3} m_j \dot{\boldsymbol{r}}_j + \sum_{j=1}^{3} m_j \dot{\boldsymbol{r}}_j \cdot \dot{\boldsymbol{r}}_j \Bigg] \tag{5}$$

The second term is zero because of the c.m. constraint, and the first term is the contribution of the orbital motion to the kinetic energy. Hence, the kinetic energy can be expressed in the form

$$\begin{aligned} \mathcal{T} = {} & \tfrac{1}{2} m R_O^2 \omega^2 + \tfrac{1}{2} m \Big\{ \mu_1(\mu_2 + \mu_3) \big[\dot{l}_1^2 + l_1^2 (\dot{\theta}_1 + \omega)^2 \big] \\ & + \mu_3(\mu_1 + \mu_2) \big[\dot{l}_2^2 + l_2^2 (\dot{\theta}_2 + \omega)^2 \big] \\ & + 2\mu_1\mu_3 [\dot{l}_1 l_2 (\dot{\theta}_2 + \omega) - l_1 \dot{l}_2 (\dot{\theta}_1 + \omega)] \sin(\theta_1 - \theta_2) \\ & + 2\mu_1\mu_3 [\dot{l}_1 \dot{l}_2 + l_1 l_2 (\dot{\theta}_1 + \omega)(\dot{\theta}_2 + \omega)] \cos(\theta_1 - \theta_2) \Big\} \end{aligned} \tag{6}$$

where ω is the orbital angular velocity of the center of mass. The potential energy is due to gravity and is given by

$$\mathcal{V} = -\sum_{j=1}^{3} \frac{\mu m_j}{|\boldsymbol{R}_O + \boldsymbol{r}_j|} \tag{7}$$

Equation (7) may be approximated by expanding it into a binomial series and keeping terms up to $O(1/R_O^3)$:

$$\begin{aligned} \mathcal{V} &\approx -\sum_{j=1}^{3} \frac{\mu m_j}{R_O} + \sum_{j=1}^{3} \frac{\mu m_j x_j}{R_O^2} + \sum_{j=1}^{3} \frac{\mu m_j}{2R_O^3} \big(x_j^2 + y_j^2 - 3x_j^2 \big) \\ &= -\sum_{j=1}^{3} m_j \omega^2 R_O^2 + \sum_{j=1}^{3} \frac{m_j}{2} \omega^2 \big(y_j^2 - 2x_j^2 \big) \end{aligned} \tag{8}$$

where Eq. (1) and $\omega = \sqrt{(\mu/R_O^3)}$ have been employed. Equation (8) can be expressed in terms of the generalized coordinates as

$$\begin{aligned} \mathcal{V} = {} & -\sum_{j=1}^{3} m_j \omega^2 R_O^2 + \frac{1}{2} m \omega^2 \Big\{ \mu_1(\mu_2 + \mu_3) l_1^2 \big(1 - 3\cos^2\theta_1 \big) \\ & + \mu_3(\mu_1 + \mu_2) l_2^2 \big(1 - 3\cos^2\theta_2 \big) + 2\mu_1\mu_3 l_1 l_2 [\cos(\theta_1 - \theta_2) \\ & - 3\cos\theta_1 \cos\theta_2] \Big\} \end{aligned} \tag{9}$$

Lagrange's equations may be applied in a relatively straightforward manner:

$$\frac{\mathrm{d}}{\mathrm{d}t} \left(\frac{\partial \mathcal{T}}{\partial \dot{q}_j} \right) - \frac{\partial \mathcal{T}}{\partial q_j} + \frac{\partial \mathcal{V}}{\partial q_j} = Q_{q_j} \tag{10}$$

After performing the required differentiations, the equations of motion can be expressed as

$$\begin{aligned} & m\mu_1(\mu_2 + \mu_3) l_1^2 \big[\ddot{\theta}_1 + 2(\dot{l}_1/l_1)(\dot{\theta}_1 + \omega) + 3\omega^2 \sin\theta_1 \cos\theta_1 \big] \\ & + m\mu_1\mu_3 l_1 l_2 \Big\{ 3\omega^2 \sin\theta_1 \cos\theta_2 + [\ddot{\theta}_2 + 2(\dot{l}_2/l_2)(\dot{\theta}_2 + \omega)] \\ & \times \cos(\theta_1 - \theta_2) + \big[(\dot{\theta}_2 + \omega)^2 - \omega^2 - (\ddot{l}_2/l_2) \big] \sin(\theta_1 - \theta_2) \Big\} \\ & = Q_{\theta_1} \end{aligned} \tag{11}$$

$$\begin{aligned} & m\mu_3(\mu_1 + \mu_2) l_2^2 \big[\ddot{\theta}_2 + 2(\dot{l}_2/l_2)(\dot{\theta}_2 + \omega) + 3\omega^2 \sin\theta_2 \cos\theta_2 \big] \\ & + m\mu_1\mu_3 l_1 l_2 \Big\{ 3\omega^2 \cos\theta_1 \sin\theta_2 + \big[\ddot{\theta}_1 + 2(\dot{l}_1/l_1)(\dot{\theta}_1 + \omega) \big] \\ & \times \cos(\theta_1 - \theta_2) + \big[\omega^2 - (\dot{\theta}_1 + \omega)^2 + (\ddot{l}_1/l_1) \big] \sin(\theta_1 - \theta_2) \Big\} \\ & = Q_{\theta_2} \end{aligned} \tag{12}$$

$$\begin{aligned} & m\mu_1(\mu_2 + \mu_3) \Big\{ \ddot{l}_1 - l_1 \big[(\dot{\theta}_1 + \omega)^2 + \omega^2 \big(3\cos^2\theta_1 - 1 \big) \big] \Big\} \\ & + m\mu_1\mu_3 \Big\{ [\ddot{l}_2 - l_2 \dot{\theta}_2 (\dot{\theta}_2 + 2\omega)] \cos(\theta_1 - \theta_2) \\ & + [l_2 \ddot{\theta}_2 + 2\dot{l}_2 (\dot{\theta}_2 + \omega)] \sin(\theta_1 - \theta_2) - 3\omega^2 l_2 \cos\theta_1 \cos\theta_2 \Big\} \\ & = Q_{l_1} \end{aligned} \tag{13}$$

$$\begin{aligned} & m\mu_3(\mu_1 + \mu_2) \Big\{ \ddot{l}_2 - l_2 \big[(\dot{\theta}_2 + \omega)^2 + \omega^2 \big(3\cos^2\theta_2 - 1 \big) \big] \Big\} \\ & + m\mu_1\mu_3 \Big\{ [\ddot{l}_1 - l_1 \dot{\theta}_1 (\dot{\theta}_1 + 2\omega)] \cos(\theta_1 - \theta_2) \\ & - [l_1 \ddot{\theta}_1 + 2\dot{l}_1 (\dot{\theta}_1 + \omega)] \sin(\theta_1 - \theta_2) - 3\omega^2 l_1 \cos\theta_1 \cos\theta_2 \Big\} \\ & = Q_{l_2} \end{aligned} \tag{14}$$

The generalized forces are due to the nonconservative control tensions, which may be evaluated using the principle of virtual work,

$$Q_{q_j} = (\boldsymbol{T}_1 - \boldsymbol{T}_3) \cdot \frac{\partial \boldsymbol{r}_1}{\partial q_j} + (\boldsymbol{T}_2 - \boldsymbol{T}_1) \cdot \frac{\partial \boldsymbol{r}_2}{\partial q_j} + (\boldsymbol{T}_3 - \boldsymbol{T}_2) \cdot \frac{\partial \boldsymbol{r}_3}{\partial q_j} \tag{15}$$

where the tension force vectors are defined by

$$\boldsymbol{T}_1 = T_1(\cos\theta_1, \sin\theta_1), \qquad \boldsymbol{T}_2 = T_2(\cos\theta_2, \sin\theta_2)$$

$$\boldsymbol{T}_3 = (T_3/l_3)(-l_1\cos\theta_1 - l_2\cos\theta_2, -l_1\sin\theta_1 - l_2\sin\theta_2) \quad (16)$$

where $l_3 = \sqrt{[l_1^2 + l_2^2 + 2l_1l_2\cos(\theta_1 - \theta_2)]}$ is the length of the third tether. From these expressions the generalized forces may be obtained as

$$Q_{\theta_1} = T_3[l_1l_2\sin(\theta_1 - \theta_2)/l_3], \qquad Q_{\theta_2} = -T_3[l_1l_2\sin(\theta_1 - \theta_2)/l_3]$$

$$Q_{l_1} = -T_1 - (T_3/l_3)[l_1 + l_2\cos(\theta_1 - \theta_2)]$$

$$Q_{l_2} = -T_2 - (T_3/l_3)[l_2 + l_1\cos(\theta_1 - \theta_2)] \quad (17)$$

Notice that the simple three-mass open configuration can be simulated by simply setting $T_3 = 0$.

Nondimensional Equations

From a numerical point of view, it is more convenient to express the equations of motion in nondimensional form. This is accomplished by changing the independent variable from time to the nondimensional time $\tau = \omega t$ and introducing the nondimensional tether lengths as $\Lambda_j = l_j/L$, $j = 1, 2, 3$, where L is the reference length for the tethers when fully deployed. Denoting the nondimensional time derivative as $()' = \mathrm{d}/\mathrm{d}\tau$, the equations of motion can be expressed as

$$\mu_1(\mu_2 + \mu_3)\Lambda_1^2[\theta_1'' + 2(\Lambda_1'/\Lambda_1)(\theta_1' + 1) + 3\sin\theta_1\cos\theta_1]$$
$$+ \mu_1\mu_3\Lambda_1\Lambda_2\{3\sin\theta_1\cos\theta_2 + [\theta_2'' + 2(\Lambda_2'/\Lambda_2)(\theta_2' + 1)]$$
$$\times \cos(\theta_1 - \theta_2) + [(\theta_2' + 1)^2 - 1 - (\Lambda_2''/\Lambda_2)]\sin(\theta_1 - \theta_2)\}$$
$$= (u_3/\Lambda_3)\Lambda_1\Lambda_2\sin(\theta_1 - \theta_2) \quad (18)$$

$$\mu_3(\mu_1 + \mu_2)\Lambda_2^2[\theta_2'' + 2(\Lambda_2'/\Lambda_2)(\theta_2' + 1) + 3\sin\theta_2\cos\theta_2]$$
$$+ \mu_1\mu_3\Lambda_1\Lambda_2\{3\cos\theta_1\sin\theta_2 + [\theta_1'' + 2(\Lambda_1'/\Lambda_1)(\theta_1' + 1)]$$
$$\times \cos(\theta_1 - \theta_2) + [1 - (\theta_1' + 1)^2 + (\Lambda_1''/\Lambda_1)]\sin(\theta_1 - \theta_2)\}$$
$$= -(u_3/\Lambda_3)\Lambda_1\Lambda_2\sin(\theta_1 - \theta_2) \quad (19)$$

$$\mu_1(\mu_2 + \mu_3)\{\Lambda_1'' - \Lambda_1[(\theta_1' + 1)^2 + (3\cos^2\theta_1 - 1)]\} + \mu_1\mu_3$$
$$\times \{[\Lambda_2'' - \Lambda_2\theta_2'(\theta_2' + 2)]\cos(\theta_1 - \theta_2) + [\Lambda_2\theta_2'' + 2\Lambda_2'(\theta_2' + 1)]$$
$$\times \sin(\theta_1 - \theta_2) - 3\Lambda_2\cos\theta_1\cos\theta_2\}$$
$$= -u_1 - (u_3/\Lambda_3)[\Lambda_1 + \Lambda_2\cos(\theta_1 - \theta_2)] \quad (20)$$

$$\mu_1(\mu_2 + \mu_3)\{\Lambda_2'' - \Lambda_2[(\theta_2' + 1)^2 + (3\cos^2\theta_2 - 1)]\}$$
$$+ \mu_1\mu_3\{[\Lambda_1'' - \Lambda_1\theta_1'(\theta_1' + 2)]\cos(\theta_1 - \theta_2)$$
$$+ [\Lambda_1\theta_1'' + 2\Lambda_1'(\theta_1' + 1)]\sin(\theta_1 - \theta_2) - 3\Lambda_1\cos\theta_1\cos\theta_2\}$$
$$= -u_2 - (u_3/\Lambda_3)[\Lambda_2 + \Lambda_1\cos(\theta_1 - \theta_2)] \quad (21)$$

where $u_j = T_j/(m\omega^2L)$, $j = 1, 2, 3$, are the nondimensional control tensions.

Control Tensions

The problem of controlling tethered satellite systems using tension control is not a straightforward task. In fact, solving optimal control problems using shooting methods for such systems is extremely difficult because of the sensitivity of the control tension to small perturbations. Although this can be avoided by using direct methods, problems inevitably arise when trying to validate solutions because even small errors in the control tension lead to errors in the length dynamics, and eventually the system diverges from the determined trajectory.[28] In Ref. 28, it was demonstrated that this problem can be alleviated by specifying the control tension as a function of the commanded length Λ_c. This idea can naturally be extended to the control of a tethered formation by specifying the tensions in the form

$$u_j = u_{0_j} + k_{1_j}(\Lambda_j - \Lambda_{c_j}) + k_{2_j}\Lambda_j', \qquad j = 1, 2, 3 \quad (22)$$

where u_{0_j} is the tension required for zero-length acceleration of the jth tether and k_{1_j}, k_{2_j} are constant control gains. Essentially, then, the control problem becomes one of optimizing the commanded lengths to achieve the desired mission objectives. Alternatively, one can simply find the optimal tensions and subsequently solve for the equivalent commanded length using Eq. (22). The latter approach is used in this paper. Note that Eq. (22) is a kind of feedback linearization of the length dynamics, designed to make the tension more robust for length tracking. Equation (22) is not designed for tracking of the tether librations, which would need to be handled by a more advanced feedback controller. In this paper, the control of the tether librations is achieved by an open-loop optimal control scheme. The benefit of specifying the tension in the form given by Eq. (22) is that it is possible to numerically simulate the system with fixed length tethers, that is, station-keeping configurations. It is also possible to obtain the tensions required to keep the formation in the desired configuration.

Equation (22) is deceptively simple. In reality, the u_{0_j} terms are complicated functions of the system-state variables. To find these expressions it is necessary to solve for the u_j tensions from Eqs. (18–21) such that the tethers are not accelerating in the length direction. After decoupling the accelerations of the generalized coordinates in Eqs. (18–21), two equations are obtained for Λ_1'' and Λ_2''. An additional equation is necessary for Λ_3'', which can be obtained by differentiating the geometric relationship

$$\Lambda_3 = \sqrt{\Lambda_1^2 + \Lambda_2^2 + 2\Lambda_1\Lambda_2\cos(\theta_1 - \theta_2)} \quad (23)$$

$$\Lambda_3' = [\Lambda_1\Lambda_1' + \Lambda_2\Lambda_2' + \Lambda_1'\Lambda_2\cos(\theta_1 - \theta_2) + \Lambda_1\Lambda_2'\cos(\theta_1 - \theta_2)$$
$$- \Lambda_1\Lambda_2(\theta_1' - \theta_2')\sin(\theta_1 - \theta_2)]/\Lambda_3 \quad (24)$$

$$\Lambda_3'' = \{\Lambda_1'^2 + \Lambda_1''[\Lambda_1 + \Lambda_2\cos(\theta_1 - \theta_2)] + \Lambda_2'^2$$
$$+ \Lambda_2''[\Lambda_2 + \Lambda_1\cos(\theta_1 - \theta_2)] + 2\Lambda_1'\Lambda_2'\cos(\theta_1 - \theta_2)$$
$$- 2(\Lambda_1'\Lambda_2 + \Lambda_1\Lambda_2')(\theta_1' - \theta_2')\sin(\theta_1 - \theta_2) - \Lambda_1\Lambda_2(\theta_1'' - \theta_2'')$$
$$\times \sin(\theta_1 - \theta_2) - \Lambda_1\Lambda_2(\theta_1' - \theta_2')^2\cos(\theta_1 - \theta_2) - \Lambda_3'^2\}/\Lambda_3 \quad (25)$$

The required tension expressions are obtained by solving for the second derivatives of the generalized coordinates from Eqs. (18–21) and using Eq. (25) with $\Lambda_1'' = \Lambda_2'' = \Lambda_3'' = 0$. The resulting set of equations can be solved for the unknown tensions:

$$u_{0_1} = \{[(\mu_1\mu_3\Lambda_2^3\Lambda_3 + \mu_1\mu_3\Lambda_1^2\Lambda_2\Lambda_3 + \mu_2\mu_3\Lambda_2^3\Lambda_3)$$
$$\times \sin(\theta_1 - \theta_2)\cos(\theta_1 - \theta_2) - 2\mu_1\mu_3\Lambda_1\Lambda_2^2\Lambda_3\sin^3(\theta_1 - \theta_2)$$
$$+ (2\mu_1\mu_3 + \mu_2\mu_3)\Lambda_1\Lambda_2^2\Lambda_3\sin(\theta_1 - \theta_2)]R_{\theta_1}$$
$$+ [-(\mu_1\mu_2\Lambda_1^2\Lambda_2\Lambda_3 + 2\mu_1\mu_3\Lambda_1^2\Lambda_2\Lambda_3)\sin(\theta_1 - \theta_2)$$
$$\times \cos(\theta_1 - \theta_2) - (\mu_1\mu_3\Lambda_1^3\Lambda_3 + \mu_1\mu_2\Lambda_1^3\Lambda_3 + \mu_1\mu_3\Lambda_1\Lambda_2^2\Lambda_3)$$
$$\times \sin(\theta_1 - \theta_2)]R_{\theta_2} + [\mu_1\mu_3\Lambda_1\Lambda_2^3\Lambda_3 + \mu_1\mu_3\Lambda_1^3\Lambda_2\Lambda_3$$
$$+ \mu_1\mu_2\Lambda_1^3\Lambda_2\Lambda_3 + \mu_2\mu_3\Lambda_1\Lambda_2^3\Lambda_3 + 2\mu_1\mu_3\Lambda_1^2\Lambda_2^2\Lambda_3$$
$$\times \cos(\theta_1 - \theta_2)]\sin^2(\theta_1 - \theta_2)R_{\Lambda_1} - \mu_1\mu_2\mu_3\Lambda_1\Lambda_2\gamma_1[\mu_2\Lambda_1$$

$$+\mu_3\Lambda_1+\mu_1\Lambda_1\cos^2(\theta_1-\theta_2)+\mu_1\Lambda_2\cos(\theta_1-\theta_2)$$
$$+\mu_2\Lambda_2\cos(\theta_1-\theta_2)+\mu_3\Lambda_2\cos(\theta_1-\theta_2)\big]\big\}\big/\gamma_2 \quad (26)$$

$$u_{0_2}=\big\{\big[\big(\mu_1\mu_3\Lambda_2^3\Lambda_3+\mu_1\mu_3\Lambda_1^2\Lambda_2\Lambda_3+\mu_2\mu_3\Lambda_2^3\Lambda_3\big)\sin(\theta_1-\theta_2)$$
$$+\big(\mu_2\mu_3\Lambda_1\Lambda_2^2\Lambda_3+2\mu_1\mu_3\Lambda_1\Lambda_2^2\Lambda_3\big)\sin(\theta_1-\theta_2)\cos(\theta_1-\theta_2)\big]$$
$$\times R_{\theta_1}+\big[-\big(\mu_1\mu_2\Lambda_1^3\Lambda_3+\mu_1\mu_3\Lambda_1^3\Lambda_3+\mu_1\mu_3\Lambda_1\Lambda_2^2\Lambda_3\big)$$
$$\times\sin(\theta_1-\theta_2)\cos(\theta_1-\theta_2)-\big(\mu_1\mu_2\Lambda_1^2\Lambda_2\Lambda_3+2\mu_1\mu_3\Lambda_1^2\Lambda_2\Lambda_3\big)$$
$$\times\sin(\theta_1-\theta_2)+2\mu_1\mu_3\Lambda_1^2\Lambda_2\Lambda_3\sin^3(\theta_1-\theta_2)\big]R_{\theta_2}$$
$$+\big[\big(\mu_1\mu_3\Lambda_1\Lambda_2^3\Lambda_3+\mu_1\mu_3\Lambda_1^3\Lambda_2\Lambda_3+\mu_1\mu_2\Lambda_1^3\Lambda_2\Lambda_3$$
$$+\mu_2\mu_3\Lambda_1\Lambda_2^3\Lambda_3\big)\sin^2(\theta_1-\theta_2)+2\mu_1\mu_3\Lambda_1^2\Lambda_2^2\Lambda_3\sin^2(\theta_1-\theta_2)$$
$$\times\cos(\theta_1-\theta_2)\big]R_{\Lambda_2}-\mu_1\mu_2\mu_3\Lambda_1\Lambda_2\gamma_1\big[\mu_1\Lambda_2+\mu_2\Lambda_2$$
$$+\mu_3\Lambda_1\cos(\theta_1-\theta_2)+\mu_1\Lambda_1\cos(\theta_1-\theta_2)+\mu_2\Lambda_1$$
$$\times\cos(\theta_1-\theta_2)+\mu_3\Lambda_2\cos^2(\theta_1-\theta_2)\big]\big\}\big/\gamma_2 \quad (27)$$

$$u_{0_3}=\big\{\big[-\mu_1\mu_3\Lambda_1\Lambda_2\Lambda_3\sin(\theta_1-\theta_2)\cos(\theta_1-\theta_2)-\big(\mu_1\mu_3\Lambda_2^2\Lambda_3$$
$$+\mu_2\mu_3\Lambda_2^2\Lambda_3\big)\sin(\theta_1-\theta_2)\big]R_{\theta_1}+\big[\big(\mu_1\mu_3\Lambda_1^2\Lambda_3+\mu_1\mu_2\Lambda_1^2\Lambda_3\big)$$
$$\times\sin(\theta_1-\theta_2)+\mu_1\mu_3\Lambda_1\Lambda_2\Lambda_3\sin(\theta_1-\theta_2)\cos(\theta_1-\theta_2)\big]R_{\theta_2}$$
$$+\mu_1\mu_3\Lambda_1\Lambda_2\gamma_1\big[\mu_1\mu_2+\mu_1\mu_3-\mu_1\mu_3\cos^2(\theta_1-\theta_2)+\mu_2^2$$
$$+\mu_2\mu_3\big]\big\}\Lambda_3\big/\gamma_2 \quad (28)$$

where the following terms have been defined:

$$\gamma_1=\big[\Lambda_1'^2+\Lambda_2'^2-2(\Lambda_1'\Lambda_2+\Lambda_1\Lambda_2')(\theta_1'-\theta_2')\sin(\theta_1-\theta_2)$$
$$+2\Lambda_1'\Lambda_2'\cos(\theta_1-\theta_2)-\Lambda_1\Lambda_2(\theta_1'-\theta_2')^2\cos(\theta_1-\theta_2)$$
$$-\Lambda_3'^2\big]\big/\Lambda_3 \quad (29)$$

$$\gamma_2=\Lambda_1\Lambda_2\Lambda_3\sin^2(\theta_1-\theta_2)\big[\mu_1\mu_3\Lambda_1^2+\mu_1\mu_2\Lambda_1^2+\mu_1\mu_3\Lambda_2^2$$
$$+\mu_2\mu_3\Lambda_2^2+2\mu_1\mu_3\Lambda_1\Lambda_2\cos(\theta_1-\theta_2)\big] \quad (30)$$

$$R_{\theta_1}=-\mu_1(\mu_2+\mu_3)\Lambda_1^2[2(\Lambda_1'/\Lambda_1)(\theta_1'+1)+3\sin\theta_1\cos\theta_1]$$
$$+3\sin\theta_1\cos\theta_2-\mu_1\mu_3\Lambda_1\Lambda_2\big\{2(\Lambda_2'/\Lambda_2)(\theta_2'+1)$$
$$\times\cos(\theta_1-\theta_2)+\big[(\theta_2'+1)^2-1\big]\sin(\theta_1-\theta_2)\big\} \quad (31)$$

$$R_{\theta_2}=-\mu_3(\mu_1+\mu_2)\Lambda_2^2[2(\Lambda_2'/\Lambda_2)(\theta_2'+1)+3\sin\theta_2\cos\theta_2]$$
$$+3\cos\theta_1\sin\theta_2-\mu_1\mu_3\Lambda_1\Lambda_2\big\{2(\Lambda_1'/\Lambda_1)(\theta_1'+1)$$
$$\times\cos(\theta_1-\theta_2)+\big[1-(\theta_1'+1)^2\big]\sin(\theta_1-\theta_2)\big\} \quad (32)$$

$$R_{\Lambda_1}=\mu_1(\mu_2+\mu_3)\big\{\Lambda_1\big[(\theta_1'+1)^2+\big(3\cos^2\theta_1-1\big)\big]\big\}+\mu_1\mu_3$$
$$\times\{\Lambda_2\theta_2'(\theta_2'+2)\cos(\theta_1-\theta_2)-[2\Lambda_2'(\theta_2'+1)]\sin(\theta_1-\theta_2)$$
$$+3\Lambda_2\cos\theta_1\cos\theta_2\} \quad (33)$$

$$R_{\Lambda_2}=\mu_1(\mu_2+\mu_3)\big\{\Lambda_2\big[(\theta_2'+1)^2+\big(3\cos^2\theta_2-1\big)\big]\big\}+\mu_1\mu_3$$
$$\times\{\Lambda_1\theta_1'(\theta_1'+2)\cos(\theta_1-\theta_2)-[2\Lambda_1'(\theta_1'+1)]\sin(\theta_1-\theta_2)$$
$$+3\Lambda_1\cos\theta_1\cos\theta_2\} \quad (34)$$

Optimal Control of Spinning Tethered Formations

The major goal of this work is to demonstrate effective control of the tether formation using tension control. Although control laws could be derived using various techniques such as Lyapunov's second method, among others, it is generally difficult to ascertain the performance of such controllers from the point of view of the system dynamics. Although the system has been modeled as consisting of rigid tethers, it is important to realize that in reality the tethers are elastic and capable of both longitudinal and lateral oscillations. Therefore, it is preferable to control as well as assess performance of the system relative to some prescribed criterion. Furthermore, for deployment and retrieval operations it usually most important to ensure that the system ends up in the correct configuration. Hence, we must also ensure that certain boundary conditions are satisfied. In other words, the control problem(s) can best be formulated within the framework of optimal control.

Optimal Control Problem and Direct Solution Methods

The general family of optimal control problems considered in this paper can be stated thusly: find the state-control pair $[\boldsymbol{x}(t), \boldsymbol{u}(t)]$ that minimize the performance index

$$\mathcal{J}=\mathcal{E}[\boldsymbol{x}(t_f), t_f]+\int_{t_0}^{t_f}\mathcal{L}[\boldsymbol{x}(t), \boldsymbol{u}(t), t]\,\mathrm{d}t \quad (35)$$

subject to the nonlinear state equations

$$\dot{\boldsymbol{x}}(t)=\boldsymbol{f}(\boldsymbol{x}(t), \boldsymbol{u}(t), t) \quad (36)$$

the end-point conditions

$$\boldsymbol{e}_L^0\le\boldsymbol{e}[\boldsymbol{x}(t_0), t_0]\le\boldsymbol{e}_U^0 \quad (37)$$

$$\boldsymbol{e}_L^f\le\boldsymbol{e}[\boldsymbol{x}(t_f), t_f]\le\boldsymbol{e}_U^f \quad (38)$$

path constraints

$$\boldsymbol{g}_L\le\boldsymbol{g}[\boldsymbol{x}(t), \boldsymbol{u}(t), t]\le\boldsymbol{g}_U \quad (39)$$

and box constraints

$$\boldsymbol{x}_L\le\boldsymbol{x}(t)\le\boldsymbol{x}_U, \qquad \boldsymbol{u}_L\le\boldsymbol{u}(t)\le\boldsymbol{u}_U \quad (40)$$

where $\boldsymbol{x}\in\mathbb{R}^{n_x}$ are the state variables, $\boldsymbol{u}\in\mathbb{R}^{n_u}$ are the control inputs, $t\in\mathbb{R}$ is the time, $\mathcal{E}:\mathbb{R}^{n_0}\times\mathbb{R}\to\mathbb{R}$ is the Mayer component of cost function—that is, the terminal, nonintegral cost in Eq. (35), $\mathcal{L}:\mathbb{R}^{n_x}\times\mathbb{R}^{n_u}\times\mathbb{R}\to\mathbb{R}$ is the Bolza component of the cost function—that is, the integral cost in Eq. (35), $\boldsymbol{e}_L^0\in\mathbb{R}^{n_x}\times\mathbb{R}\to\mathbb{R}^{n_0}$ and $\boldsymbol{e}_U^0\in\mathbb{R}^{n_x}\times\mathbb{R}\to\mathbb{R}^{n_0}$ are the lower and upper bounds on the initial-point conditions, $\boldsymbol{e}_L^f\in\mathbb{R}^{n_x}\times\mathbb{R}\to\mathbb{R}^{n_f}$ and $\boldsymbol{e}_U^f\in\mathbb{R}^{n_x}\times\mathbb{R}\to\mathbb{R}^{n_f}$ are the lower and upper bounds on the final-point conditions, and $\boldsymbol{g}_L\in\mathbb{R}^{n_x}\times\mathbb{R}^{n_u}\times\mathbb{R}\to\mathbb{R}^{n_g}$ and $\boldsymbol{g}_U\in\mathbb{R}^{n_x}\times\mathbb{R}^{n_u}\times\mathbb{R}\to\mathbb{R}^{n_g}$ are the lower and upper bounds on the path constraints. The solution of general optimal control problems requires the application of Pontryagin's maximum principle[29] (PMP) to construct the necessary conditions for optimality. The PMP essentially requires that the control Hamiltonian, defined as a function of "undetermined" covectors, be minimized. This (indirect) approach, apart from being cumbersome for complex problems, produces a two-point boundary-value problem that is regarded as very difficult to solve.[30] In addition to this, the necessary conditions must be rederived for each different cost function that is considered. Instead of following this approach, it is much more efficient and convenient to apply direct transcription methods to solve the optimal control problem.[31]

The solution of optimal control problems via direct methods is well known, and several different methods are described in Ref. 31. There are a wide variety of solution methods available, most of which are based on sequential quadratic programming (SQP) algorithms for solving the underlying nonlinear programming (NLP) problem. Essentially, the state equations and cost function are discretized at a set of points along the trajectory, and the state equations

are enforced through simple integration or differentiation rules. Although the general methodology involved with each method is the same, the underlying structure of the NLP and corresponding solution accuracy can be quite different. Some examples of different discretizations that can be used are the Hermite–Simpson,[32] fifth-order Hermite–Legendre–Gauss–Lobatto,[33] and pseudospectral methods.[34,35] Despite the fact that these methods have been used routinely for a number of years, there is still no general agreement as to which method is better or even if a method can be defined as "best." Hence, there are no general guidelines available for selecting an appropriate method. There are a variety of issues that must be considered, however, when employing different methods. These relate to the possibility of bang–bang controls, singular arcs, and second-order state-control constraints. Unfortunately, when applying direct methods, these possibilities are not known a priori and must be discovered by examining numerical solutions.

A general reusable software package for solving single- (and multiple-) phase optimal control problems called DIRECT[36] has been developed by the author. The package uses the MATLAB® environment to formulate the cost function, state equations, boundary conditions, and path constraints. The problem is automatically converted into an appropriate NLP depending on the selected discretization method. The NLP is solved using the sparse sequential quadratic programming software SNOPT,[37] originally coded in Fortran but called from MATLAB via a mex-file interface. The sparse Jacobian structures for each of the discretization methods are automatically provided to SNOPT by the DIRECT software. In the numerical results, the Hermite–Simpson method has been employed for the discretization.

Applicability of the Optimal Maneuvers

Control of the tether formation is assumed to be achieved exclusively via tension control. Tension control is used in conjunction with reel mechanisms to reel in and reel out the tethers. It is much more desirable to control the tension instead of the tether-length rate because it is necessary to maintain the tether tension above zero (i.e., slack tether condition). However, actual control of the system spin rate is achieved by the interaction of variable length tethers in the orbital frame, which generates Coriolis forces that are able to do work against the gravity gradient. Hence, the method employed here to control the system spin is generally only applicable where the orbital angular velocity is sufficient (i.e., low Earth orbits). Although the results are expressed nondimensionally and the maneuvers could be potentially performed at much higher orbital altitudes and around other central bodies, the maneuver times would also be much longer. Furthermore, the maneuvers are generally not applicable for formations at the sun–Earth L_2 point because of the assumption of a low Earth orbit. Control of similar tether formations at these other locations is an important avenue for future work. Finally, it must be noted that the changes in system configuration and spin rate are not achieved for "free" but require energy to be expended in reeling the tethers. This energy is assumed to come from solar energy collected by the satellites and stored in batteries for use by the tether winches.

Numerical Results

Optimal control of the tethered formation is studied for a variety of different scenarios. To begin, some relatively simple minimum-time configuration changes are considered, such as an increase in spin rate and shape change. Deployment and retrieval operations are then considered in detail. In all cases, the optimal solutions were validated by propagating the interpolated controls (using the commanded length form of tension with $k_1 = 100$, $k_2 = 10$) and comparing the results with those obtained via the direct method. Because the propagated solutions and the direct solutions are indistinguishable at the level of the plot, only the direct solutions are shown. In addition, only equal mass configurations are considered so that $\mu_1 = \mu_2 = \mu_3 = \frac{1}{3}$.

It is useful to consider the key differences between control of a tethered formation and its simpler two-body counterpart. Two-body tether systems are usually desired to be deployed along the orbit local vertical for circular orbits or into periodic librational solutions when elliptical orbits are considered. However, such deployed configurations are not possible for a triangular tethered formation because it requires that one tether sustain compressive forces, which is clearly impractical. In contrast, a tethered formation requires a relatively high spin rate to maintain stability. For single-tether systems, such spinning scenarios tend to be avoided (except for momentum-exchange architectures) because of fear of the tether wrapping around the mother satellite. In other words, the techniques commonly used for control of two-body tethered systems are not applicable to tethered formation flying. This has implications both in terms of the specification of the boundary conditions for deployment and retrieval as well as cost-function selection.

Configuration Changes

One important class of maneuvers is the minimum-time reorientation or reconfiguration of a tethered formation. Although such maneuvers are not preferable using tension control because of the bang–bang nature of the solutions, they are important because they represent the lower limit in which a given maneuver can be executed. For numerical solutions obtained for the minimum-time-performance criterion, the nondimensional tension was limited within the range $u \in [0.01, 2]$ for each of the tethers.

Increase in Spin Rate

A potentially useful maneuver for a spinning tethered formation is to increase the spin rate of the system without the use of tangential thrusters. This is possible by utilizing the Coriolis forces generated by the system as the tether lengths change. This technique has been demonstrated successfully for single-tethered systems and is a critical feature that allows control of the system librations. However, the extension to tethered formation flying is not straightforward or intuitive. Therefore, the first scenario that is considered in this paper is to simply pump the tether spin rate. For this case, it is desirable to perform the maneuver in minimum time. For illustrative purposes the following problem has been defined:

$$\mathcal{J} = \min \tau_f \tag{41}$$

subject to

$$[\theta_1 - \theta_2, \theta_1', \theta_2', \Lambda_1, \Lambda_2, \Lambda_1', \Lambda_2']_{\tau=0} = [-120\,\text{deg}, 1, 1, 1, 1, 0, 0]$$

$$[\theta_1 - \theta_2, \theta_1', \theta_2', \Lambda_1, \Lambda_2, \Lambda_1', \Lambda_2']_{\tau=\tau_f} = [-120\,\text{deg}, 3, 3, 1, 1, 0, 0] \tag{42}$$

In this problem it is desired to increase the spin rate from 1 revolution per orbit to 3 revolutions per orbit. Note that the boundary conditions for the tether angles are specified in terms of the relative angle of tethers 1 and 2, and the value is based on the requirement to maintain the desired configuration determined from the equation

$$\theta_1 - \theta_2 = -\cos^{-1}\frac{\Lambda_3^2 - \Lambda_1^2 - \Lambda_2^2}{2\Lambda_1\Lambda_2} \tag{43}$$

This means that the actual orientation of the system with respect to the orbital frame at the beginning and end of the maneuver is free to be optimized.

The minimum time for this maneuver was determined to be approximately 1.503 rad of nondimensional time, or approximately one quarter of an orbit. For a 500-km-altitude orbit, this would equate to roughly 22–23 min in real time. Figure 2 shows projections of the tether formation in the orbital frame during the maneuver, with the initial and final configurations labeled. This clearly illustrates the large variation in the system geometry during the maneuver. Figure 3 shows the time histories of the tether states and controls. As expected, the tension control input is of a bang–bang nature, and no singular arcs appear to be present in the solution. When the tension is on the lower bound, this generally correlates to a positive change in the tether-length rate. Alternatively, when the tension is on the upper bound, the reel acceleration is negative. The effect of the length rate on the librational motion of the tethers is similar to

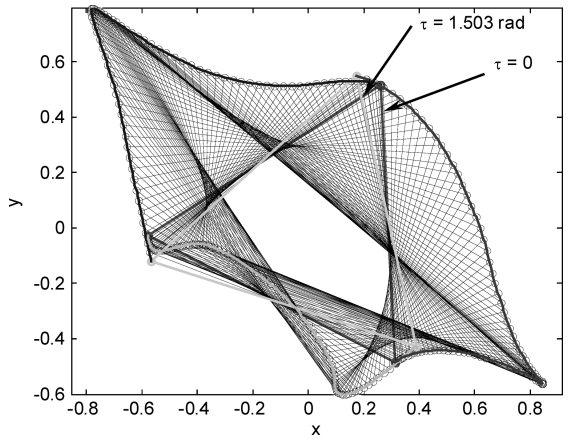

Fig. 2 Projections of tether configuration during minimum-time spin-rate increase.

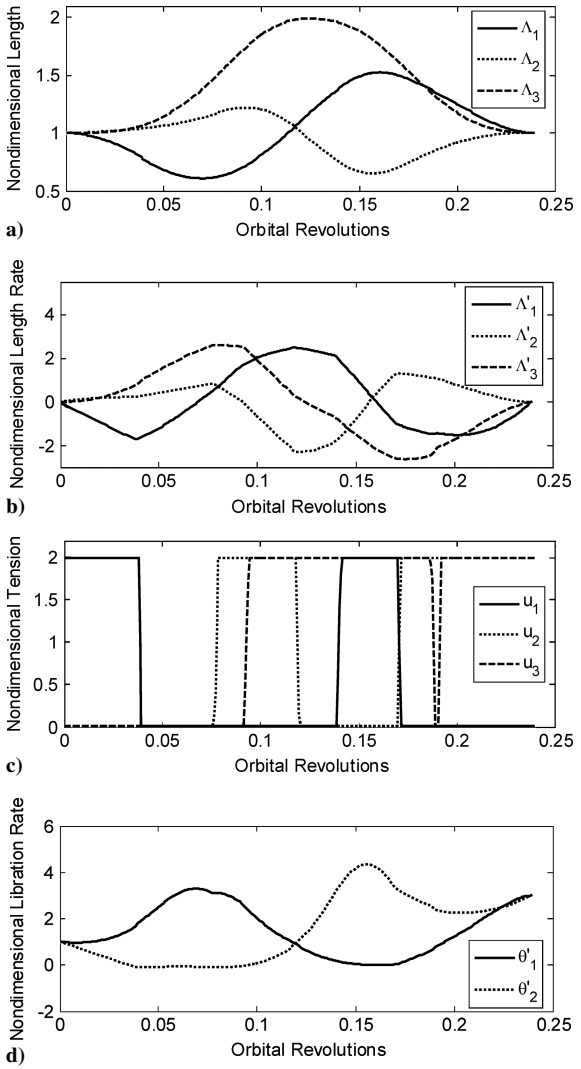

Fig. 3 Minimum-time spin-rate increase: a) length, b) length rate, c) tension, and d) libration rate.

the effect of tension on the length rate. When the length rate is positive, there tends to be a decrease in the change in libration rate such that the librational acceleration is negative. On the other hand, negative length rates correlate with positive librational accelerations, and hence, the length rate tends to be negative near the end of the maneuver for the spin-up case. An examination of the length variations demonstrates some apparent symmetry in the maneuver. Tether 1 is first reeled in, then reeled out, and then reeled in again, whereas tether 2 is reeled out, then reeled in, and then reeled out. The variation in length of the third tether is more severe because it is reeled out and then reeled in only. Its length varies by up to twice its original length for this particular maneuver, whereas tether 1 varies in the range of (−40%, +53%) and tether 2 varies in the range of (−35%, +22%). The maximum nondimensional reel rates for each of the tethers lie in the ranges of $\Lambda_1' \in [-1.70, 2.50]$, $\Lambda_2' \in [-2.26, 1.30]$, and $\Lambda_3' \in [-2.60, 2.62]$. If a 500-km-altitude orbit is assumed for the system, then for every 1 km of reference tether length, one unit of nondimensional length rate translates to approximately 1.107 m/s in dimensional units. Hence, for a 10-km nominal tether length, this maneuver would require reels capable of generating up to 30 m/s in reel rate. The libration rates also show quite large variations from the initial rate(s) to the final rate(s). The libration rate of tethers 1 and 2 both go to zero during the maneuver. In other words, the minimum-time maneuver does not simply increase the spin rate in a uniform or nearly uniform manner. It is evident that the formation does not rotate at a common rate and that it undergoes a rather large distortion to increase the spin rate to the desired amount. This indicates the complex interaction between the Coriolis forces and changes in the configuration.

Decrease in Spin Rate

The second maneuver that is considered is a despin case combined with a shape change. The minimum-time maneuver is determined so as to satisfy the boundary conditions

$$[\theta_1 - \theta_2, \theta_1', \theta_2', \Lambda_1, \Lambda_2, \Lambda_1', \Lambda_2']_{\tau=0} = [-120\,\text{deg}, 3, 3, 1, 1, 0, 0]$$

$$[\Lambda_3, \theta_1', \theta_2', \Lambda_1, \Lambda_2, \Lambda_1', \Lambda_2']_{\tau=\tau_f} = [1.5, 1, 1, 1, 1, 0, 0] \quad (44)$$

These boundary conditions essentially require the tether formation be reconfigured from an equilateral shape to an isosceles shape with the third tether length equal to 1.5 times the length of tethers 1 and 2. This boundary condition is actually implemented via the difference in libration angles as determined via Eq. (43) because the length of the third tether is not a state variable. The minimum time for this particular maneuver was determined to be 1.011 rad or approximately 16% of one orbit. Numerical results are presented in Figs. 4 and 5.

Figure 4 shows projections of the tether formation during the despin maneuver. The variation in the shape of the formation is much less pronounced than for the spin-up case (compare Fig. 4 with Fig. 2). This is because the maneuver time is shorter and generally, for a decrease in spin rate one would expect an increase in tether length. Hence, the desired increase in length of the third tether also helps to decrease the system spin rate. Figure 5 again illustrates the bang–bang nature of the control tension as well as the general smaller variations of the system states compared with the spin-up maneuver shown in Fig. 3. The overall variations in tether length and length rate appear to be smaller in general than for the previous

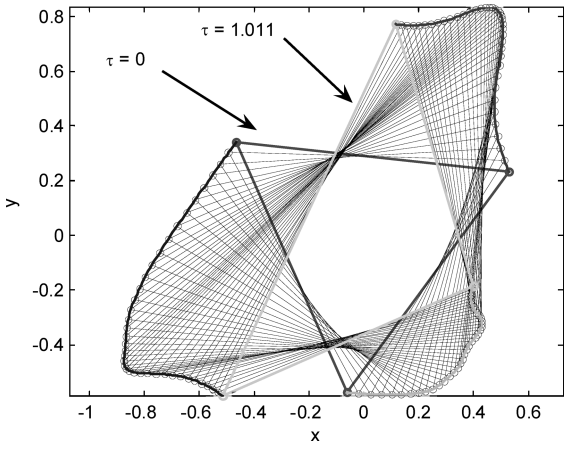

Fig. 4 Projections of tether configuration during minimum-time spin-rate decrease.

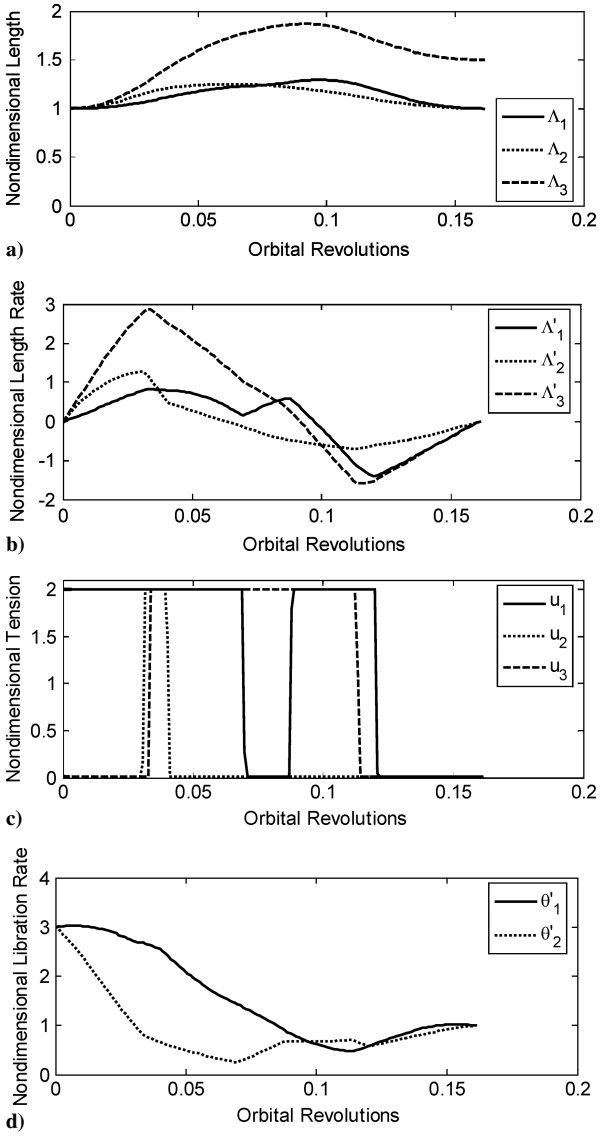

Fig. 5 Minimum-time spin-rate decrease: a) length, b) length rate, c) tension, and d) libration rate.

case. In addition, the length variation follows a distinctly different trend then the previous results. For example, all of the tethers are reeled out first and then reeled in. The maximum length variation of tether 1 is on the order of 30%, whereas tether 2 varies by about 25%, and tether 3 varies by roughly 87%. These variations are significantly less severe than the previous results. Furthermore, the libration rates of tethers 1 and 2 do not go to zero during this maneuver, nor does the libration rate increase in the first stages of the maneuver. The maximum nondimensional reel rates for each of the tethers lie in the ranges of $\Lambda_1' \in [-1.41, 0.84]$, $\Lambda_2' \in [-0.71, 1.28]$, and $\Lambda_3' \in [-1.57, 2.87]$. For nominal 10-km-long tethers, a reel capable of generating up to a 32-m/s reel rate would be needed.

Deployment Trajectories

The minimum-time maneuvers considered in the previous section show nonsmooth variations in the control tension and rapid changes in the tether-length rate. These phenomena can lead to undesirable features in flexible tethers such as longitudinal and lateral vibrations and should be avoided by appropriate selection of the performance index. For two-body tethered systems, various performance indices were compared by Williams and Trivailo,[38] and it was found that minimizing the reel acceleration of the tether consistently produces trajectories that give smooth variations in the system states. However, for a spinning tethered formation such a performance index alone does not necessarily give a desirable trajectory. One must also account for the fact that the configuration is closed and therefore there is the potential for tether collisions. Therefore, it is also desirable to minimize the distortion to the configuration from the equilateral reference triangle. Hence, the cost function is selected as the sum of components from the angular accelerations as well as length accelerations:

$$\mathcal{J} = \int_{\tau_0}^{\tau_f} \left\{ W_1 \left[(\theta_1'')^2 + (\theta_2'')^2 \right] + W_2 \left[(\Lambda_1'')^2 + (\Lambda_2'')^2 + (\Lambda_3'')^2 \right] \right\} \mathrm{d}\tau \tag{45}$$

where W_1 and W_2 are weighting coefficients. Because the terms in the performance index are nondimensional, the weights have been selected as $W_1 = W_2 = 1$. Note that one could weight the contributions differently if one wanted to keep the system rotation rate as close to being constant as possible rather than minimizing the effective control input. However, it is the minimization of the length accelerations that gives smooth variations in the control tensions and length dynamics. Different weightings are a design choice, and different choices would lead to differences in the overall nature of the results. For the sake of brevity, only results for $W_1 = W_2 = 1$ are presented in this paper.

As noted previously, it is important to restrict the tethers from physically coming into contact with each other. To ensure this, bounds are placed on the tether lengths and libration angles such that

$$\Lambda_1 \geq 0.01, \qquad \Lambda_2 \geq 0.01 \tag{46}$$

$$-179 \leq \theta_1 - \theta_2 \leq -1 \,\text{deg} \tag{47}$$

This ensures that no two tethers cross each other, as can be seen by examining the system geometry. This constraint becomes active for deployment and retrieval when the system spin rate is high. Without this constraint, crossing of tethers occurs in the optimal solutions.

The boundary conditions for deployment have been selected as

$$\begin{aligned} &[\theta_1 - \theta_2, \theta_1', \theta_2', \Lambda_1, \Lambda_2, \Lambda_1', \Lambda_2']_{\tau=0} \\ &\quad = [-120\,\text{deg}, \theta_d', \theta_d', 0.1, 0.1, 0, 0] \\ &[\theta_1 - \theta_2, \theta_1', \theta_2', \Lambda_1, \Lambda_2, \Lambda_1', \Lambda_2']_{\tau=\tau_f} \\ &\quad = [-120\,\text{deg}, \theta_d', \theta_d', 1, 1, 0, 0] \end{aligned} \tag{48}$$

where θ_d' is the desired system spin rate. Hence, the deployment requires that there be no net change in the tether spin rate.

An issue that arises when applying the boundary conditions defined by Eq. (48) is whether the system final conditions are maintained because of possible nonzero accelerations after the completion of the maneuver. This is generally not an issue when the controller is switched to the station-keeping controller defined by simply setting the commanded tether lengths to $\Lambda_{c_j} = 1$, $j = 1, 2, 3$, after the maneuver is completed. This causes a small jump in the control tensions and has a negligible effect on the system motion. One possible alternative is to employ the additional boundary conditions

$$[\theta_1'', \theta_2'', \Lambda_1'', \Lambda_2'']_{\tau=\tau_f} = [0, 0, 0, 0] \tag{49}$$

as well as switching to the station-keeping controller. However, the numerical results with these boundary conditions show negligible differences in the complete maneuver compared to the strategy discussed previously. Compressive or bending forces are not required from the tethers because of the centrifugal stiffening caused by the high system rotation rate. Therefore, in the results, the constraints due to Eq. (49) are not used and only the optimal maneuver dynamics are shown.

One- and two-orbit deployment trajectories have been determined for desired spin rates of two, five, and eight revolutions per orbit. Numerical results for two revolutions per orbit deployment are shown in Figs. 6–8. Figure 6 shows projections of the tether configuration during one-orbit deployment, Fig. 7 shows projections for the two-orbit deployment, and Fig. 8 shows the corresponding state and control trajectories. Figure 6 illustrates the variation in system geometry

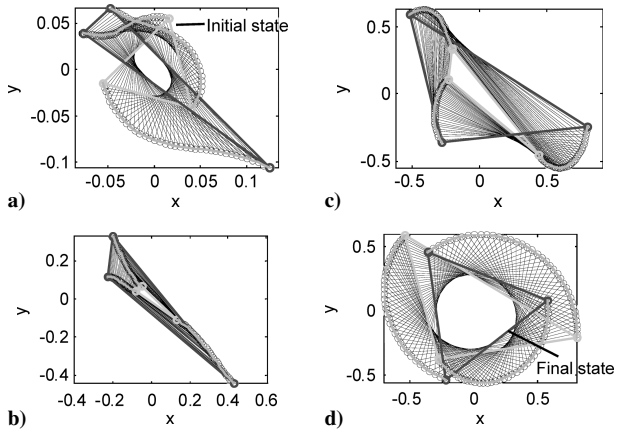

Fig. 6 Projections of tether configuration during one-orbit deployment for two revolutions per orbit spin rate: a) first quarter orbit, b) second quarter orbit, c) third quarter orbit, and d) final quarter orbit.

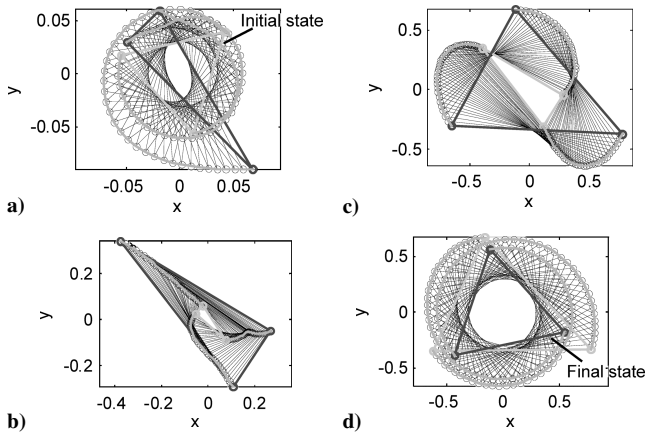

Fig. 7 Projections of tether configuration during two-orbit deployment for two revolutions per orbit spin rate: a) first half orbit, b) second half orbit, c) first half of second orbit, and d) second half of second orbit.

during the deployment. This plot highlights the general nature of the optimal deployment of such a tether formation. Initially, the system is spinning at the desired rate, but the initial deployment of tether causes the spin rate to decrease. The main proportion of the deployment occurs with the system in an isosceles-triangular configuration at a nearly constant angle to the local vertical. Hence, the system emulates closely the traditional two-body configuration during deployment. Here, one tether remains relatively short compared with the other two tethers. This effectively allows the system to make use of gravity-gradient effects during deployment. The two longer tethers generally tend to be deployed beyond the desired length. The system then reels the tethers back to the correct length while the third tether is reeled out, timed so that the final spin rate is achieved. Figure 7 shows the projections of the system for two-orbit deployment. This plot illustrates that the two-orbit deployment trajectories are similar to the one-orbit deployment trajectories in the sense that the majority of the deployment takes place with the system close to zero libration rate. The major difference in the two-orbit case is that the system keeps the tether lengths short for nearly a quarter of the total deployment time. The corresponding state and control trajectories for both one- and two-orbit deployment are shown in Fig. 8. Figure 8 demonstrates that there is generally less reeling required to achieve the desired deployment configuration for two-orbit deployment than for one-orbit deployment. For the one-orbit deployment case, both tethers 1 and 2 are deployed in excess of the desired length by about 10%, whereas the third tether is deployed an extra 58%. The nondimensional length rates are in the ranges $\Lambda_1' \in [-0.16, 0.57]$, $\Lambda_2' \in [-0.09, 0.46]$, and $\Lambda_3' \in [-0.5, 0.64]$. These reeling requirements are much less severe than was observed for the minimum-time

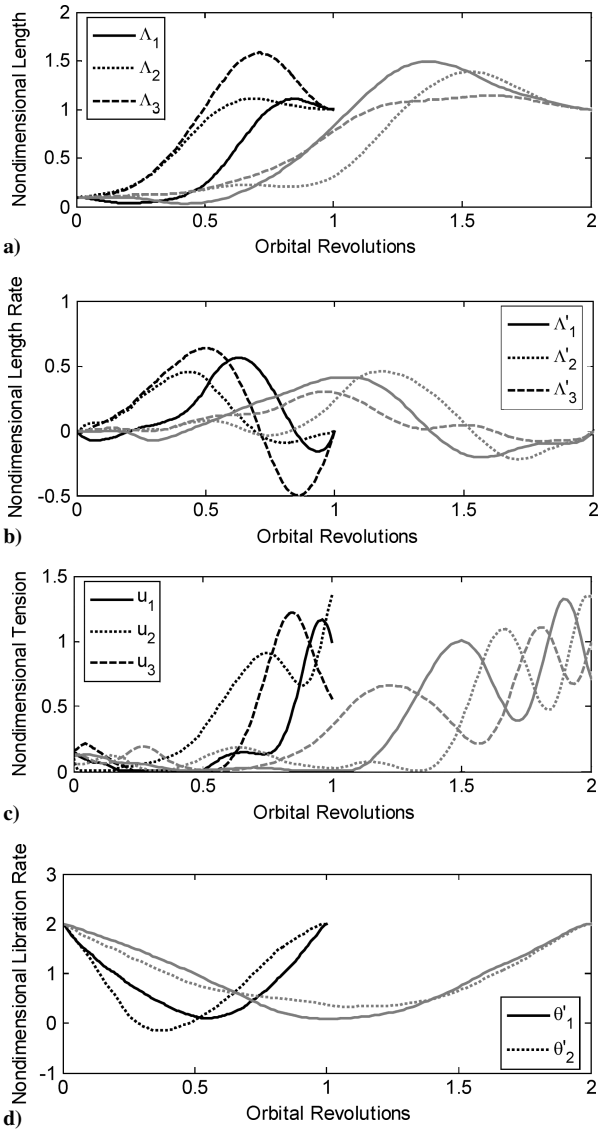

Fig. 8 Deployment trajectories for two revolutions per orbit spin rate (black, one orbit; gray, two orbit): a) length, b) length rate, c) tension, and d) libration rate.

maneuvers. For a 10-km tether, the maximum reel-rate requirement is on the order of 7 m/s. As one might expect, allowing two orbits to complete the deployment tends to decrease the length-rate requirements. Tether 1 is deployed an extra 49% beyond the desired length, tether 2 38%, and tether 3 14%. The nondimensional length rates for two-orbit deployment lie in the ranges $\Lambda_1' \in [-0.20, 0.41]$, $\Lambda_2' \in [-0.22, 0.46]$, and $\Lambda_3' \in [-0.08, 0.30]$, the maximum of which is about 5 m/s in dimensional units for a 10-km tether. The libration rates appear to vary in a parabolic-like fashion, approaching minima of zero approximately midway through the total deployment time. The minima correspond to the peaks in the tether deployment rate. It can also be seen that the libration rates are different for the one-orbit deployment, indicating distortion of the system geometry, but are more comparable during the two-orbit deployment. The control tensions, shown in Fig. 8c, vary in a very smooth manner but are clipped at the lower limit several times during the deployment.

Numerical results for deployment for a spin rate of five revolutions per orbit are shown in Figs. 9–11. Figure 9 shows projections of the system for one-orbit deployment. The nature of the deployment is very similar for this spin rate as for the previous case. That is, the deployment tends to take place with the system in an elongated triangular shape at a nearly constant angle to the local vertical. The higher spin rate means that it is necessary to deploy the tethers to approximately twice the desired length and then to

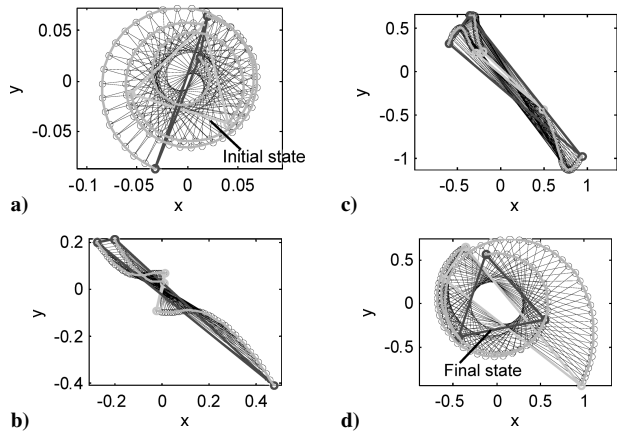

Fig. 9 Projections of tether configuration during one-orbit deployment for five revolutions per orbit spin rate: a) first quarter orbit, b) second quarter orbit, c) third quarter orbit, and d) final quarter orbit.

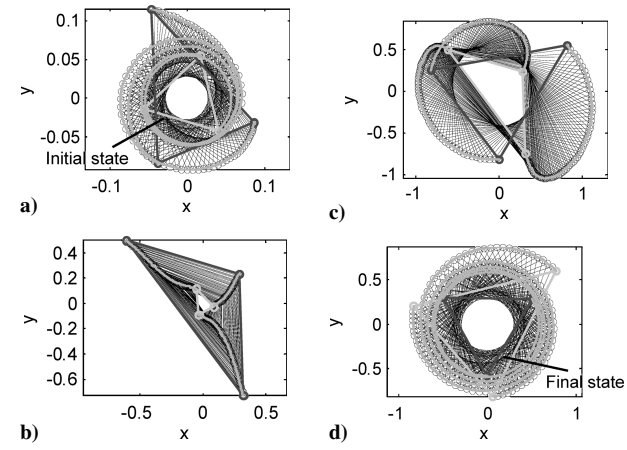

Fig. 10 Projections of tether configuration during two-orbit deployment for five revolutions per orbit spin rate: a) First half orbit, b) second half orbit, c) first half of second orbit, and d) second half of second orbit.

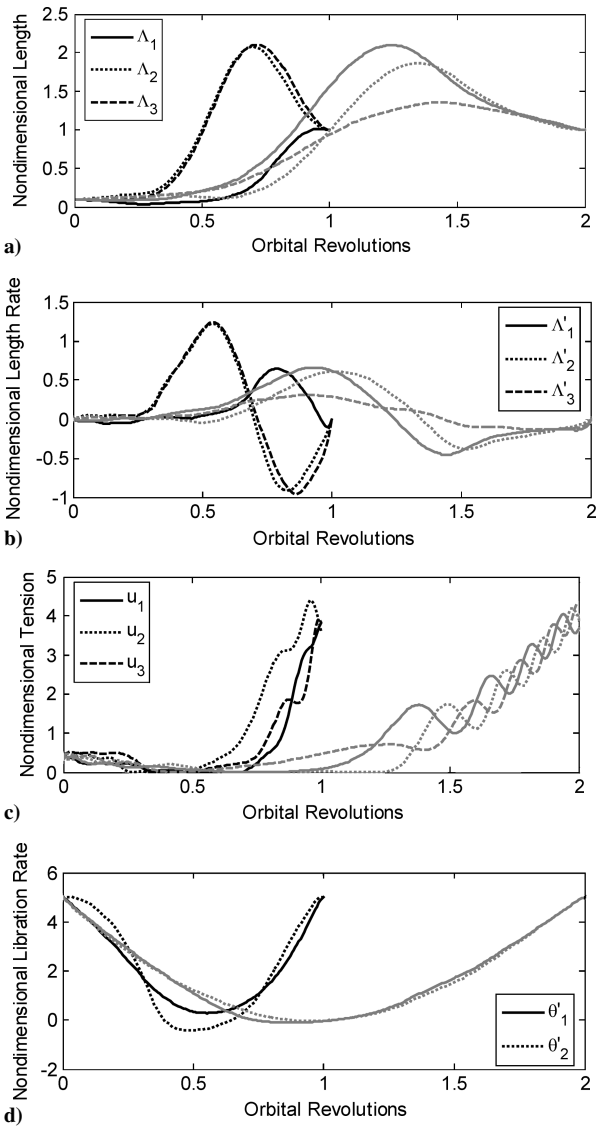

Fig. 11 Deployment trajectories for five revolutions per orbit spin rate (black, one orbit; gray, two orbit): a) length, b) length rate, c) tension, and d) libration rate.

retrieve them rapidly. This can be seen clearly in Figs. 9c and 9d. Figure 10 shows projections of the system for the same spin-rate deployment but for two orbits. Figure 10b shows that the system is not as elongated as in the previous cases. Figure 10d shows that the spin rate is increased gradually by pulling in the tethers over several rotations of the system, as opposed to the rapid retrieval necessary for one-orbit deployment (Fig. 9d). For one-orbit deployment, tethers 2 and 3 are deployed in an almost identical fashion, as can be seen by examining the length and length rate variations (Figs. 11a and 11b). The control tensions, however, are not the same because of the influence of the gravity gradient, as well as the control tension from the first tether. The results show that tether 1 is first reeled in, where it is held for nearly three quarters of the orbit, after which it is reeled out to the desired length with minimal excess of deployed tether. Tethers 2 and 3, on the other hand, are deployed to about 2.07 and 2.10 times the desired length, respectively, before being reeled in. The nondimensional length rates for one-orbit deployment are in the ranges $\Lambda_1' \in [-0.10, 0.65]$, $\Lambda_2' \in [-0.91, 1.22]$, and $\Lambda_3' \in [-0.95, 1.24]$, the maximum of which is about 13.7 m/s for a 10-km tether. The deployment trajectories for two-orbit deployment are quite different to the one-orbit case. Tether 1 is deployed to 2.09 times the desired length, whereas tethers 2 and 3 are deployed 87% and 36% in excess of the desired length, respectively. All of the tethers are reeled in at the end of the maneuver. Doubling the total maneuver time again reduces the required peak length rates. The nondimensional length rates for two-orbit deployment are in the ranges $\Lambda_1' \in [-0.45, 0.67]$, $\Lambda_2' \in [-0.38, 0.61]$, and $\Lambda_3' \in [-0.13, 0.31]$, the maximum of which is about 7.4 m/s for a 10-km tether. Hence, a nearly 50% reduction in the peak length rate is achieved. The libration rates show trends similar to those of the previous cases; that is, it tends to decrease to almost zero during the main portion of the deployment and is increased when the tether is retrieved from the overdeployed position. The libration rates are nearly equal for the two-orbit deployment case, which accounts for the nearly uniform geometry of the system shown in Fig. 10. The control tensions are shown in Fig. 11c. The cyclic variation of the control tensions toward the end of the maneuver for the two-orbit deployment case is mostly caused by the natural variation of the tension resulting from the rotation as well as gravity-gradient effects.

Deployment trajectories for a spin rate of eight revolutions per orbit are shown in Fig. 12. The general behavior of the deployment trajectories are quite similar to the previous results, except that the amount of extra deployed tether is much greater, leading to higher peak length rates. For example, for one orbit, the excess deployment lengths are 8, 129, and 179% for tethers 1, 2, and 3, respectively, whereas for two orbits, the excess deployment lengths are 143, 0, and 155%. The peak length rates are about 18 and 11 m/s for one- and two-orbit deployments, respectively, for a 10-km tether. Thus, as the system spin rate increases, the peak length rate requirements also increase, but longer deployment times decrease the peak length rate with respect to shorter deployment times.

It is clear from these results that it is possible to deploy a tether formation into a configuration with relatively high rotation rate without

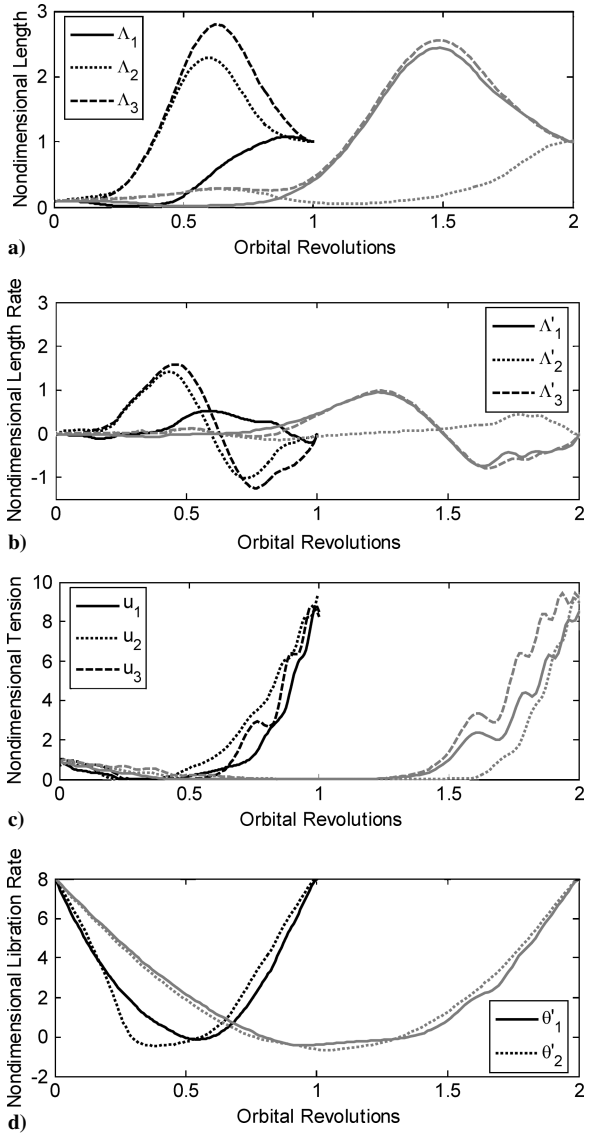

Fig. 12 Deployment trajectories for eight revolutions per orbit spin rate (black, one orbit; gray, two orbit): a) length, b) length rate, c) tension, and d) libration rate.

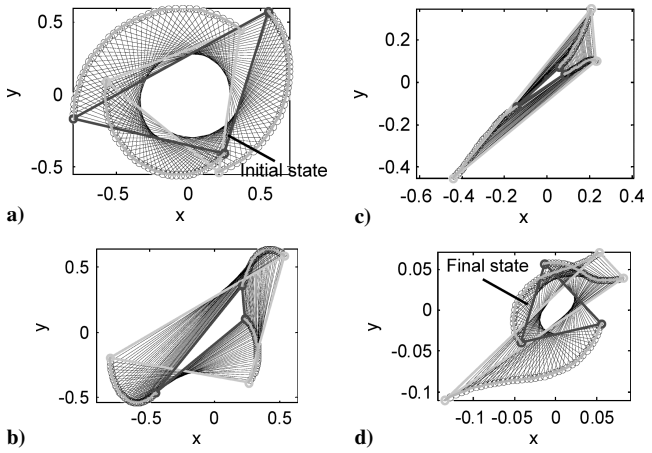

Fig. 13 Projections of tether configuration during one-orbit retrieval for two revolutions per orbit spin rate: a) first quarter orbit, b) second quarter orbit, c) third quarter orbit, and d) final quarter orbit.

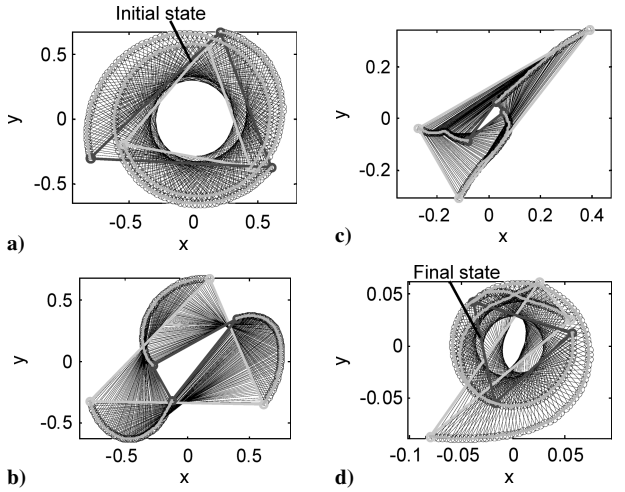

Fig. 14 Projections of tether configuration during two-orbit retrieval for two revolutions per orbit spin rate: a) first half orbit, b) second half orbit, c) first half of second orbit, and d) second half of second orbit.

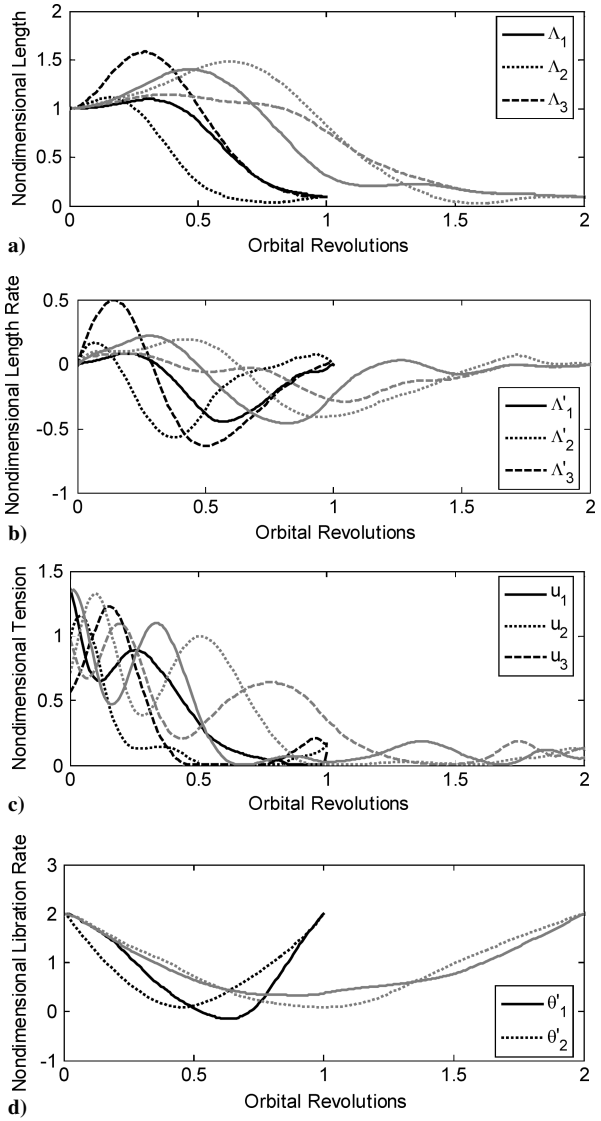

Fig. 15 Retrieval trajectories for two revolutions per orbit spin rate (black, one orbit; gray, two orbit): a) length, b) length rate, c) tension, and d) libration rate.

the use of tangential thrusters. It is also clear, however, that the technique for doing this is not intuitive and requires some relatively sophisticated control achieved via tether reeling.

Retrieval Trajectories

The boundary conditions for the retrieval trajectories were set to be the reverse of deployment. The same set of spin cases were solved as for deployment. However, for the sake of brevity, only the results from a retrieval of two revolutions per orbit are presented because of the symmetrical nature of the deployment/retrieval results. Figure 13 shows projections of the system for a retrieval of two revolutions per orbit for one orbit. A comparison of this with Fig. 6 shows the symmetry of the deployment and retrieval maneuvers. Note that Fig. 13d is the reverse of Fig. 6a, Fig. 13c is the reverse of Fig. 6b, and so on. The same pattern(s) can be seen for the two-orbit retrieval shown in Fig. 14 when compared with Fig. 7. Figure 15 shows the system state and control trajectories for retrieval. Note that a comparison of these with Fig. 8 shows the symmetry of the results, except that some of the tethers (numbering) are interchanged because the configuration is symmetric with respect to mass and geometry. Similar symmetries have been proven in the deployment/retrieval trajectories for two-body tethered systems with symmetrical boundary conditions.[38] The symmetry of the results for a tethered formation is a good validation of the numerical solutions. Hence, the optimal retrieval trajectories require the tethers to be reeled out initially and then reeled in. Simply reeling the tethers in would result in a net increase in spin rate and explains why the optimal deployment trajectories must reel the tethers out beyond the desired length for the scenarios considered here.

Conclusions

Optimal control of a spinning triangular tethered formation has been studied. A control model, treating the formation as three-point masses connected via inelastic tethers, was used to study the nature of the system trajectories. The only control inputs to the system are the tether tensions. A robust form of the tether tension control (specified in terms of commanded length variations) was derived, enabling efficient simulations of the system for variable-length or fixed-length tethers. Optimal trajectories for different maneuvers were obtained using direct transcription methods. Three maneuvers were considered: 1) minimum-time reorientation, 2) deployment, and 3) retrieval. Minimum-time reorientation maneuvers are bang–bang in the control input and demonstrate that simple spin-up and despin maneuvers can be performed in less than a quarter of an orbit with no thrust inputs. Control actuation is provided by the coupling of the tether-length variation and the orbital motion of the system. Optimal deployment/retrieval trajectories were obtained for different spin rates for both one- and two-orbit maneuver times so as to minimize a combination of the librational acceleration and length accelerations of the tethers. The optimal trajectories demonstrate a symmetry for deployment and retrieval. The results also show that deployment/retrieval is optimally performed by slowing the system spin rate and deploying/retrieving the tethers in a gravity-gradient-type manner with the system at a nearly constant angle to the local vertical. The tethers are typically overdeployed and then retrieved so as to take advantage of Coriolis accelerations to ensure that the system meets the spin-rate requirements. Overall, the results illustrate the possibilities of controlling a spinning tethered formation without consuming fuel.

References

[1]Leitner, J., Quinn, D., and Matsumura, M., "From Monolithics to Tethers to Freeflyers—The Spectrum of Large Aperture Sensing from Space," *Proceedings of SPIE, Interferometry in Space*, Vol. 4852, No. 2, 2003, pp. 492–499.

[2]Misra, A. K., and Modi, V. J., "A Survey on the Dynamics and Control of Tethered Satellite Systems," *Advances in the Astronautical Sciences*, Vol. 62, Pt. 1, 1987, pp. 667–719.

[3]Misra, A. K., Amier, Z., and Modi, V. J., "Attitude Dynamics of Three-Body Tethered Systems," *Acta Astronautica*, Vol. 17, No. 10, 1988, pp. 1059–1068.

[4]Misra, A. K., "Equilibrium Configurations of Tethered Three-Body Systems and Their Stability," *Journal of Astronautical Sciences*, Vol. 50, No. 3, 2002, pp. 241–253.

[5]Tan, Z., and Bainum, P., "Tethered Satellite Constellations in Auroral Observation Missions," AIAA Paper 2002-4640, Aug. 2002.

[6]Farley, R. E., and Quinn, D. A., "Tethered Formation Configurations—Meeting the Scientific Objectives of Large Aperture and Interferometric Science," AIAA Paper 2001-4770, Aug. 2001.

[7]Sedwick, R. J., and Schweighart, S. A., "Propellantless Spin-Up of Tethered or Electromagnetically Coupled Sparse Apertures," *Proceedings of SPIE, the International Society for Optical Engineering*, Vol. 4849, No. 1, 2002, pp. 193–204.

[8]Quadrelli, M. B., "Modeling and Dynamics Analysis of Tethered Formations for Space Interferometry," American Astronautical Society, Paper AAS 01-231, Feb. 2001.

[9]Quadrelli, M. B., "Centralized Dynamics and Control of Novel Orbiting Formation of Tethered Spacecraft," International Astronautical Federation, Paper IAC A.5.02, Oct. 2002.

[10]Quadrelli, M. B., Hadaegh, F. Y., Lorenzini, E. C., and Bombardelli, C., "Precision Tethered Formations for LEO and Space Interferometry Applications," 16th International Symposium on Space Flight Dynamics, Jet Propulsion Lab., California Inst. of Technology, Pasadena, CA, 2001.

[11]Quadrelli, M. B., Hadaegh, F. Y., Shao, M., and Lorenzini, E. C., "Formations of Tethered Spacecraft as Stable Platforms for Far IR and Sub-mm Astronomy," *Second Workshop on New Concepts for Far-Infrared and Submillimeter Space Astronomy*, NASA CP-2003-212233, 2003, pp. 472–482.

[12]Bombardelli, C., Lorenzini, E. C., and Quadrelli, M. B., "Pointing Dynamics of Tether-Controlled Formation Flying for Space Interferometry," American Astronautical Society, Paper AAS 01-404, Aug. 2001.

[13]Bombardelli, C., Lorenzini, E. C., and Quadrelli, M. B., "Dynamical Effects of Solar Radiation Pressure on a Spinning Tether System for Interferometry," American Astronautical Society, Paper AAS 04-170, Jan. 2004.

[14]Bombardelli, C., Lorenzini, E. C., and Quadrelli, M. B., "Retargeting Dynamics of a Linear Tethered Interferometer," *Journal of Guidance, Control, and Dynamics*, Vol. 27, No. 6, 2004, pp. 1061–1067.

[15]Kim, M., and Hall, C. D., "Dynamics and Control of Tethered Satellite Systems for NASA's SPECS Mission," American Astronautical Society, Paper AAS 03-532, Aug. 2003.

[16]Quinn, D. A., and Folta, D. C., "A Tethered Formation Flying Concept for the SPECS Mission," American Astronautical Society, Paper AAS 00-015, Feb. 2000.

[17]DeCou, A. B., "Tether Static Shape for Rotating Multimass, Multitether, Spacecraft 'Triangle' Michelson Interferometer," *Journal of Guidance, Control, and Dynamics*, Vol. 12, No. 2, 1989, pp. 273–275.

[18]Cosmo, M. L., Lorenzini, E. C., and Bombardelli, C., "Space Tethers as Testbeds for Spacecraft Formation-Flying," American Astronautical Society, Paper AAS 04-171, Jan. 2004.

[19]Williams, T., and Moore, K., "Dynamics of Tethered Satellite Formations," American Astronautical Society, Paper AAS 02-198, Jan. 2002.

[20]Tragesser, S., "Formation Flying with Tethered Spacecraft," AIAA Paper 2000-4133, Aug. 2000.

[21]Tragesser, S. G., and Tuncay, A., "Orbital Design of Earth-Oriented Tethered Satellite Formations," AIAA Paper 2002-4641, Aug. 2002.

[22]Pizarro-Chong, A., and Misra, A. K., "Dynamics of a Multi-Tethered Satellite Formation," AIAA Paper 2004-5308, Aug. 2004.

[23]Nakaya, K., Iai, M., Omagari, K., Yabe, H., and Matunga, S., "Formation Deployment Control for Spinning Tethered Formation Flying—Simulations and Ground Experiments," AIAA Paper 2004-4896, Aug. 2004.

[24]Fujii, H. A., and Anazawa, S., "Deployment/Retrieval Control of Tethered Subsatellite Through an Optimal Path," *Journal of Guidance, Control, and Dynamics*, Vol. 17, No. 6, 1994, pp. 1292–1298.

[25]Barkow, B., Steindl, A., Troger, H., and Wiedermann, G., "Various Methods of Controlling the Deployment of a Tethered Satellite," *Journal of Vibration and Control*, Vol. 9, No. 1, 2003, pp. 187–208.

[26]Lakso, J., and Coverstone, V. L., "Optimal Tether Deployment/Retrieval Trajectories Using Direct Collocation," AIAA Paper 2000-4349, Aug. 2000.

[27]Blanksby, C., and Trivailo, P., "Assessment of Actuation Methods for Manipulating Tip Position of Long Tethers," *Space Technology*, Vol. 20, No. 1, 2000, pp. 31–39.

[28]Williams, P., "Spacecraft Rendezvous on Small Relative Inclination Orbits Using Tethers," *Journal of Spacecraft and Rockets*, Vol. 42, No. 6, 2005, pp. 1047–1060.

[29]Sussman, H. J., and Williems, J. C., "300 Years of Optimal Control: From the Brachystochrone to the Maximum Principle," *IEEE Control Systems Magazine*, Vol. 17, No. 3, 1997, pp. 32–44.

[30]Bryson, A. E., and Ho, Y.-C., *Applied Optimal Control*, Hemisphere, New York, 1975, Chap. 7.

[31]Betts, J. T., *Practical Methods for Optimal Control Using Nonlinear Programming*, Advances in Control and Design Series, Society for Industrial and Applied Mechanics, Philadelphia, 2001, Chap. 4.

[32]Hargraves, C. R., and Paris, S. W., "Direct Trajectory Optimization Using Nonlinear Programming and Collocation," *Journal of Guidance, Control, and Dynamics*, Vol. 10, No. 4, 1987, pp. 338–342.

[33]Herman, A. L., and Conway, B. A., "Direct Optimization Using Collocation Based on High-Order Gauss–Lobatto Quadrature Rules," *Journal of Guidance, Control, and Dynamics*, Vol. 19, No. 3, 1996, pp. 592–599.

[34]Elnagar, G., Kazemi, M. A., and Razzaghi, M., "The Pseudospectral Legendre Method for Discretizing Optimal Control Problems," *IEEE Transactions on Automatic Control*, Vol. 40, No. 10, 1995, pp. 1793–1796.

[35]Ross, I. M., and Fahroo, F., "Legendre Pseudospectral Approximations of Optimal Control Problems," *Lecture Notes in Control and Information Sciences*, Vol. 295, 2003, pp. 327–342.

[36]Williams, P., "User's Guide to DIRECT Version 1.17," TR-05-03.01, Melbourne, Australia, March 2005.

[37]Gill, P. E., Murray, W., and Saunders, M. A., "SNOPT: An SQP Algorithm for Large-Scale Constrained Optimization," *SIAM Journal on Optimization*, Vol. 12, No. 4, 2002, pp. 979–1006.

[38]Williams, P., and Trivailo, P., "On the Optimal Deployment and Retrieval of Tethered Satellites," AIAA Paper 2005-4291, July 2005.

C. Kluever
Associate Editor